

A reduced crustal magnetization zone near the first observed active hydrothermal vent field on the Southwest Indian Ridge

Jian Zhu,¹ Jian Lin,² Yongshun J. Chen,¹ Chunhui Tao,³ Christopher R. German,² Dana R. Yoerger,² and Maurice A. Tivey²

Received 8 April 2010; revised 7 June 2010; accepted 17 June 2010; published 21 September 2010.

[1] Inversion of near-bottom magnetic data reveals a well-defined low crustal magnetization zone (LMZ) near a local topographic high (37°47'S, 49°39'E) on the ultraslow-spreading Southwest Indian Ridge (SWIR). The magnetic data were collected by the autonomous underwater vehicle ABE on board R/V DaYangYiHao in February–March 2007. The first active hydrothermal vent field observed on the SWIR is located in Area A within and adjacent to the LMZ at the local topographic high, implying that this LMZ may be the result of hydrothermal alteration of magnetic minerals. The maximum reduction in crustal magnetization is 3 A/M. The spatial extent of the LMZ is estimated to be at least $6.7 \times 10^4 \text{ m}^2$, which is larger than that of the LMZs at the TAG vent field on the Mid-Atlantic Ridge (MAR), as well as the Relict Field, Bastille, Dante-Grotto, and New Field vent-sites on the Juan de Fuca Ridge (JdF). The calculated magnetic moment, i.e., the product of the spatial extent and amplitude of crustal magnetization reduction is at least $-3 \times 10^7 \text{ Am}^2$ for the LMZ on the SWIR, while that for the TAG field on the MAR is $-8 \times 10^7 \text{ Am}^2$ and that for the four individual vent fields on the JdF range from -5×10^7 to $-3 \times 10^7 \text{ Am}^2$. Together these results indicate that crustal demagnetization is a common feature of basalt-hosted hydrothermal vent fields at mid-ocean ridges of all spreading rates. Furthermore, the crustal demagnetization of the Area A on the ultraslow-spreading SWIR is comparable in strength to that of the TAG area on the slow-spreading MAR. **Citation:** Zhu, J., J. Lin, Y. J. Chen, C. Tao, C. R. German, D. R. Yoerger, and M. A. Tivey (2010), A reduced crustal magnetization zone near the first observed active hydrothermal vent field on the Southwest Indian Ridge, *Geophys. Res. Lett.*, 37, L18303, doi:10.1029/2010GL043542.

1. Introduction

[2] Previous studies have shown that seafloor hydrothermal venting systems can strongly affect local crustal magnetic properties. Magnetic minerals can be altered rapidly by the corrosive fluids of hydrothermal systems [Ade-Hall *et al.*,

1971; Watkins and Paster, 1971]. High-temperature hydrothermal fluids can also cause thermal demagnetization of young mid-ocean ridge basalts, which contain titanomagnetite (TM60) that has a low Curie-point temperature (150–200°C) compared to pure magnetite (580°C) [Irving, 1970; Johnson and Atwater, 1977]. In this study, we present a detailed analysis of the near-bottom magnetic data over the first observed active high-temperature hydrothermal vent field at the ultraslow-spreading SWIR. The data were collected by the autonomous underwater vehicle ABE (Autonomous Benthic Explorer) operated by the Woods Hole Oceanographic Institution (WHOI) during the second leg of the Chinese cruise DY115-19 on board R/V DaYangYiHao in Feb.–Mar. 2007 [Tao *et al.*, 2007].

[3] The SWIR (Figure 1a) represents a major boundary separating the Africa and Antarctica plates at an ultraslow full spreading rate of about 14–16 km/M.y. [Patriat and Segoufin, 1988]. The eastern part of the SWIR is divided into three major ridge sections by the Gallieni Fracture Zone (GFZ) at 52°E and the Melville Fracture Zone (MFZ) at 61°E [Patriat and Segoufin, 1988]. West of the GFZ (Figure 1b), the mean ridge axial depth is 3,090 m, while the shallowest seafloor depth is ~1,500 m at the center of Segment 27 (white solid lines) [Sauter *et al.*, 2004]. This section is associated with strongly negative Residual Mantle Bouguer Anomalies (RMBA), indicating more robust magma supply than the SWIR to the east [Georgen *et al.*, 2001; Sauter *et al.*, 2004]. Furthermore, basalt samples indicating a relatively high degree of partial melting have also been found in this section of the SWIR [Meyzen *et al.*, 2003; Font *et al.*, 2007]. These observations strongly indicate relatively thicker crust and/or hotter mantle for this section of the SWIR.

[4] Our near-bottom magnetic survey area (Figure 1c, white box) is at the western end of Segment 28, at the base of the southern rift valley wall [Sauter *et al.*, 2004]. The entire area is located within boundaries of the Brunhes Anomaly (Figures 1b and 1c, white dashed lines) [Mendel *et al.*, 2003], implying that no reverse magnetic polarity should occur in the ABE survey area.

2. Data and Analysis

[5] Three phases of ABE survey were conducted in the study area. Near-bottom magnetic data and high-resolution bathymetry data were collected using a three-component fluxgate magnetometer and a SIMRAD SM2000 200-kHz multibeam sonar, respectively. A Phase-1 survey [German *et al.*, 2008] with ABE flying at a constant depth of 2,625 m,

¹Institute of Theoretical and Applied Geophysics, School of Earth and Space Science, Peking University, Beijing, China.

²Woods Hole Oceanographic Institution, Woods Hole, Massachusetts, USA.

³Key Laboratory of Submarine Geosciences, Second Institute of Oceanography, State Oceanic Administration, Hangzhou, China.

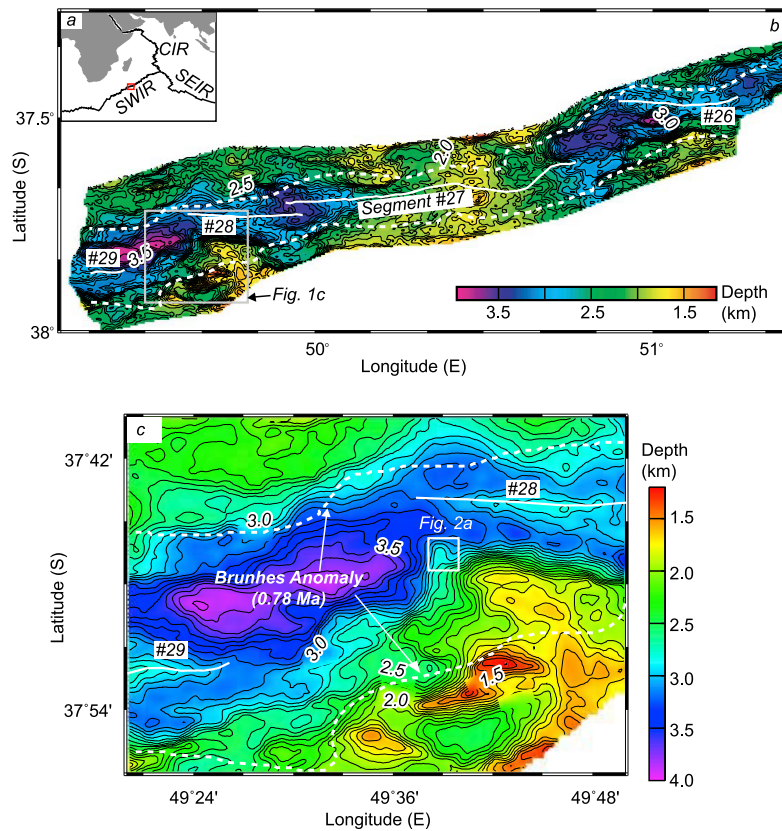


Figure 1. (a) Sketch of the location of the Southwest Indian Ridge. (b) Bathymetric map of the area within the red box shown in Figure 1a. Data were collected during the French Gallieni Cruise on board R/V L'Atalante in 1995. White dashed lines outline the boundary of the Brunhes Anomaly, and solid white lines indicate the neo-volcanic axis for the spreading segments 26 to 29 as defined by Sauter *et al.* [2004]. (c) Bathymetry of the area within the gray box in Figure 1b. The white symbols have the same meaning as those in Figure 1b, and the white box shows the working area of the ABE vehicle.

covered an area of $\sim 2.5 \text{ km} \times 2.5 \text{ km}$ with a survey line spacing of 250 m (Figure 2a, black dashed line). Total magnetic field was obtained by vector summation of the measured three-component magnetic field data. We corrected the measured magnetic field for both permanent and induced magnetic field effects of the vehicle [Tivey *et al.*, 2003] as well as Earth's regional field based on the International Geomagnetic Reference Field (IGRF) of 2005 adjusted for the survey year of 2007. The resultant magnetic field data were then interpolated onto a 50-m-spaced grid, and continued downward to a constant water-depth plane at 2,900 m, i.e., an equivalent plane [Pilkington and Urquhart, 1990; Guspi, 1987], to remove the effects of variations in vehicle altitude. The choice of 2,900 m depth led to better convergence of the Fourier transform method [Guspi, 1987]. The magnetic field data were then upward continued to a water depth of 2,650 m, since all bathymetry of the survey area lies below this depth. The final map of the magnetic field from the Phase-1 survey is shown in Figure 2b.

[6] A reduction-to-the-pole correction with the inclination of -61.9° and declination of -41.2° was made on the magnetic anomalies to eliminate the complexity caused by the non-vertical directions of both magnetization and ambient magnetic field [Blakely, 1996]. We then used the Fourier transform method of Parker and Huestis [1974] to invert magnetic field for crustal magnetization, assuming a 500-m-

thick magnetized layer with its top surface following the seafloor topography. A cosine-tapered band-pass filter with cutoff wavelengths of 6,200 m and 270 m was used to ensure the convergence of the iteration. Magnetization inversion is a non-unique process and one measure of this property is the annihilator, which is a magnetization function that produces no external magnetic field when convolved with the bathymetry [Parker and Huestis, 1974]. Since no Natural Remanent Magnetization (NRM) measurements on fresh basalt samples were currently available for the study area, we have only been able to adjust the magnetization result by adding four times the annihilator to ensure that all the magnetization values are positive within the survey area, which is a reasonable assumption given the survey location within the normal Brunhes chron. The final crustal magnetization map from the Phase-1 survey is shown in Figure 2c.

[7] Similar processing was performed on magnetic data collected during the ABE Phase-2 and Phase-3 surveys [German *et al.*, 2008]. Our Phase-2 data were collected 50 m above the seafloor with a track spacing of 30 m (Figure 2a, black solid line), while all Phase-3 data were navigated to 5 m above the seafloor with a track spacing of 10 m. We combined the calibrated magnetic data from the Phases-2 and 3 surveys after downward continuing to an equivalent level plane at 2,900 m to gain greater data coverage and bordering them with the Phase-1 magnetic data to minimize edge effects. The

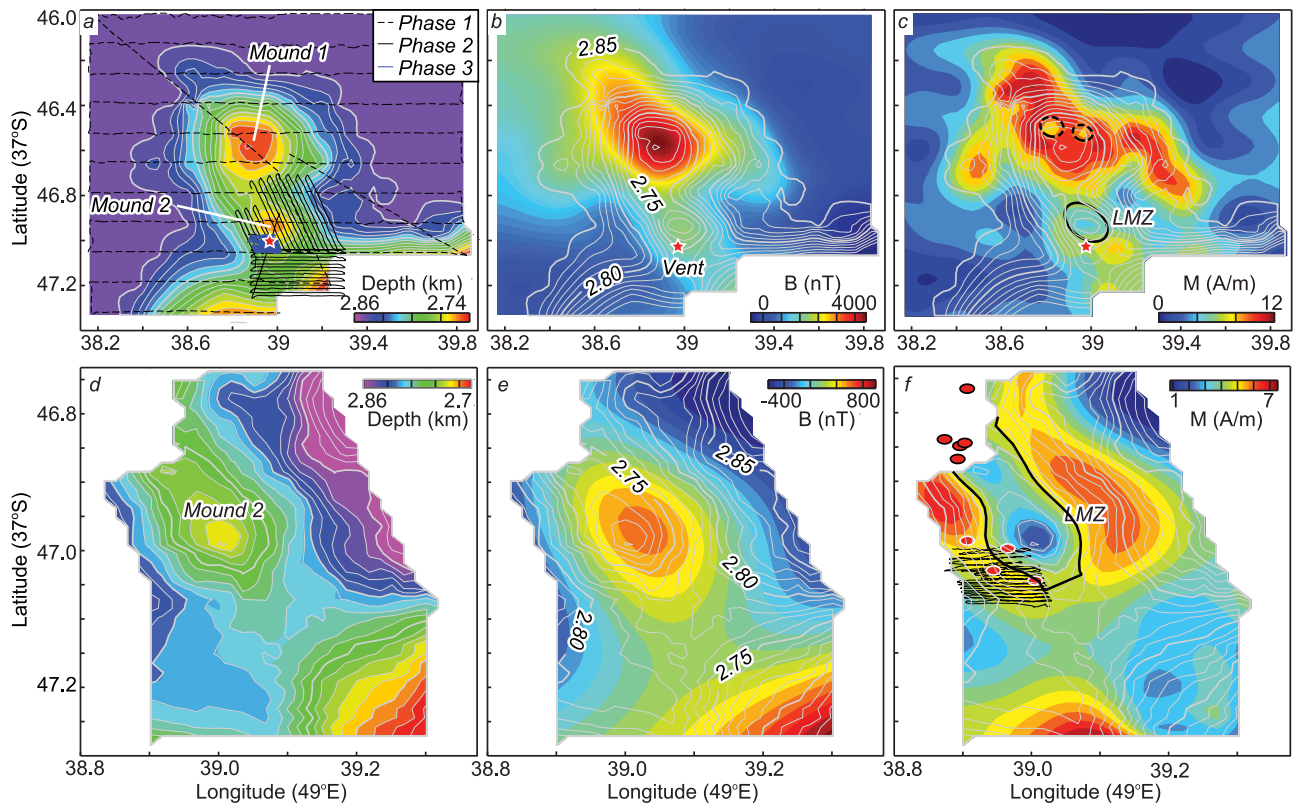


Figure 2. (a) Bathymetry, (b) near-bottom magnetic field, and (c) crustal magnetization from data collected during the ABE Phase-1 survey. Gray contours in Figures 2a–2c delineate the seafloor depth with 10-m intervals. The two sub-circular local topographic highs are labeled as Mound 1 and Mound 2. Red star indicates the location of the newly discovered high-temperature hydrothermal vent field. In Figure 2a, the track lines of the ABE Phase-1, Phase-2, and Phase-3 surveys are shown by black dashed, black solid, and blue dashed lines, respectively. The ellipses in Figure 2c indicate three low magnetization zones (LMZ) based on the result of our inversion. High resolution Phase 2 data exist only in the area outlined by the solid line. (d) Bathymetry, (e) near-bottom magnetic field, and (f) crustal magnetization from data collected during the ABE Phase-2 and Phase-3 surveys, respectively. Gray contours delineate the seafloor depth with 10-m intervals. In Figure 2f, the black ellipse indicates the area of the LMZ based on the result of our inversion. Black solid lines show the track lines of the ABE Phase-3 survey, during which bottom photographs were also obtained. Red dots represent locations at which active hydrothermal vents were discovered during the Chinese cruises DY115-19 (red ellipses with white outlines) and DY115-20 (red ellipses with black outlines).

new dataset was then continued upward to 2,650 m, again with a grid spacing of 25 m. The cutoff wavelengths of the band-pass filter for inversion were 1,600 m and 50 m. Four times the annihilator was added to the inversion solution. Final results for the magnetic field and crustal magnetization from the Phase-2 and Phase-3 surveys are shown in Figures 2e and 2f, respectively.

3. Magnetic Field and Crustal Magnetization

[8] Bathymetry within the ABE survey area shows a NNW trending topographic high with two peaks at $37^{\circ}46.6'S$, $49^{\circ}38.9'E$ (Mound 1) and $37^{\circ}47.0$, $49^{\circ}39.0'E$ (Mound 2), respectively (Figure 2a), where hydrothermal sulfide deposits and altered basaltic rocks were observed and sampled. The center of the newly observed active high-temperature hydrothermal field (red star) is located at $37^{\circ}47.02'S$ and $49^{\circ}38.95'E$ at a seafloor depth of $\sim 2,750$ m near Mound 2 [Tao *et al.*, 2007].

[9] The pattern of the magnetic field from the Phase-1 survey (Figure 2b) resembles that of the seafloor bathymetry

(Figure 2a), revealing a strong correlation between magnetic field and topography. From the results of the calculated crustal magnetization (Figure 2c), we find that the entire local topographic high is strongly magnetized compared to deeper areas, implying that this local topographic high has excess magnetic volume. In contrast, three obvious ellipse-shaped low crustal magnetization zones (LMZ, black circles on Figure 2c) are residing on these two Mounds. The most prominent LMZ with the greatest demagnetization coincides almost exactly with the crest of the smaller Mound 2 (solid black circle on Figure 2c). This LMZ has a dimension of $\sim 250 \times 400$ m² and displays a maximum reduction in magnetization of 1.5 A/m. This result implies that Mound 2 is less magnetized than Mound 1 and maybe dominated by non-magnetic hydrothermal deposits or its volcanic host rock has been substantially altered by hydrothermal processes.

[10] The magnetic field from the Phase-2 and Phase-3 surveys (Figure 2e) also shows a strong correlation with the local topography (Figure 2d). The calculated crustal magnetization (Figure 2f) shows that the whole of Mound 2 appears to be strongly magnetized around its periphery, with a well-

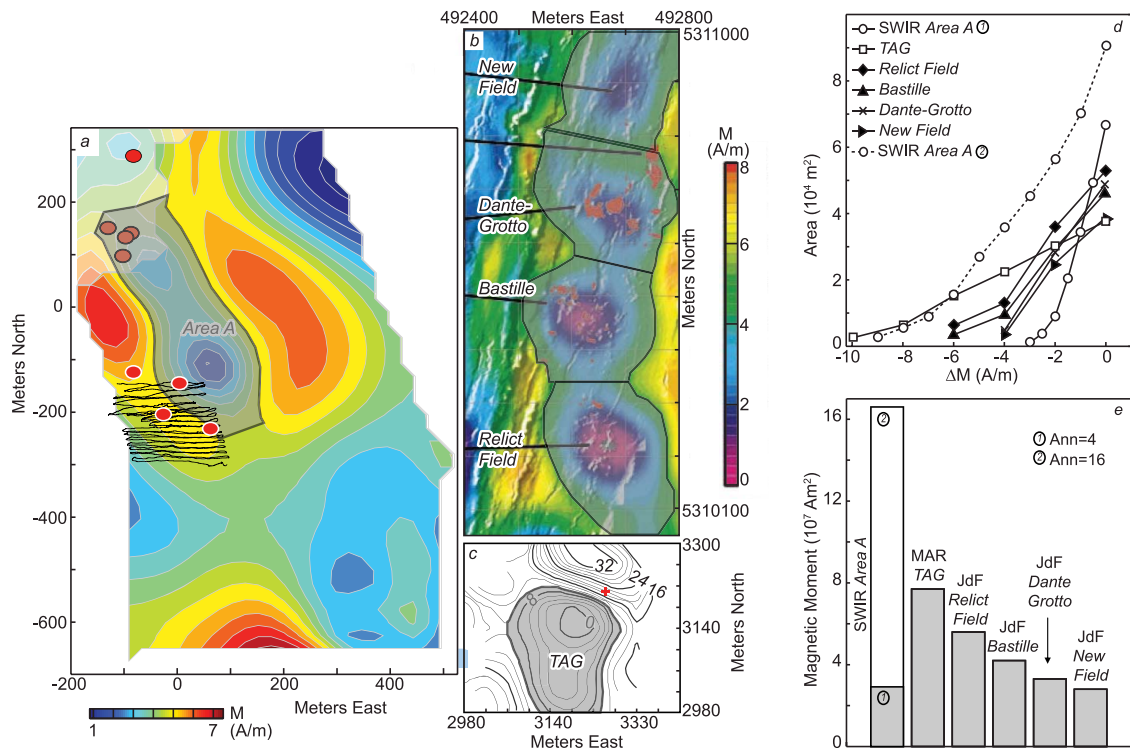


Figure 3. (left) LMZs at the (a) SWIR, (b) JdF [Tivey and Johnson, 2002], and (c) MAR [Tivey et al., 1993]. These six LMZs are named after the adjacent hydrothermal vent fields. The shapes of the LMZs are shown by grey shading. We used these interpreted LMZ areas in all calculations. Red symbols represent known hydrothermal vents. In Figure 3a, magnetization distributions in areas with dashed contours were obtained from the inversion of magnetic data from the ABE Phase-1 survey. (right) (d) Calculated areas of LMZs as a function of the reduced magnetization (ΔM) for each of the six LMZs. The values of the SWIR Area A correspond to models of 4 times annihilator (Case 1, open circles with solid line) and 16 times annihilator (Case 2, open circles with dashed line), respectively. Open squares: TAG on the MAR; filled diamonds: Relict Field on the JdF; filled triangles: Bastille on the JdF; crosses: Dante-Grotto on the JdF; and eastward filled triangles: New Field on the JdF. (e) Calculated magnetic moment, i.e., the product of the spatial extent and amplitude of crustal magnetization reduction, for each of the six LMZs. The labeled bars for the SWIR Area A show the results for the two cases mentioned in Figure 3d. Case 1 solution is regarded as the minimum value of the magnetic moment for the Area A on the SWIR.

defined LMZ extending NNW along the crest of the mound. This LMZ has a NNW trending major axis of ~ 450 m and a minor axis of ~ 150 m. The maximum magnetization reduction of this LMZ is ~ 3 A/m compared to the nearby magnetization high. Two groups of active hydrothermal vents (red dots, Figure 2f), which were discovered during two Chinese expeditions, are located within or close to this LMZ [Tao et al., 2007], suggesting that this LMZ may be the result of hydrothermal alteration associated with active high-temperature venting.

4. Magnetic Moment of Low Magnetization Zones

[11] We compared the LMZ of the SWIR Area A (this study, Figure 3a) with four vent areas of the JdF (New Field, Dante-Grotto, Bastille, and Relict Field) (Figure 3b) and the TAG area on the MAR (Figure 3c). The models of magnetization for both JdF and TAG have assumed a 500-m-thick magnetized layer and were obtained by applying enough annihilators to match the mean value of the measured Natural Remanent Magnetization (NRM) in local basaltic samples [Tivey et al., 1993; Tivey and Johnson, 2002]. To estimate the shape of the LMZ at Area A on the SWIR, we bordered the magnetization distribution of the ABE Phase-2 survey with

the data from Phase-1 (Figure 3a). For Area A on the SWIR and for TAG on the MAR, we took the contours of $M = 5$ and $M = 10$ A/m, respectively, as the outer boundaries of their LMZs; for all LMZs on the JdF, we chose the contour of $M = 6$ A/m as the outer boundary. The reduced magnetization contrast (ΔM) was obtained by subtracting the value at outer boundaries of LMZs defined above. In Figure 3d, each point on a curve shows the calculated area contained within the isopach of a ΔM value for an individual LMZ. The total LMZ area for Area A on the SWIR (Figure 3d, Case 1, highest point on the curve with open circles and solid line) is about $6.7 \times 10^4 \text{ m}^2$, which is greater than that of the TAG area on the MAR (highest point on the curve with open squares). The SWIR LMZ area is also greater than those of the four individual LMZs on the JdF (highest points on the curves with solid symbols). We also calculated a case in which sixteen times annihilator was added. The case results in the mean magnetization value within the study area to be 16 A/m, which is the same as the mean magnetization obtained from inversion at sea surface by Sauter et al. [2004]. Under this assumption (marked as Case 2 on Figure 3 (right)), the total LMZ area is $\sim 9 \times 10^4 \text{ m}^2$ (Figure 3d, highest point on the curve with open circles and dashed line).

[12] Finally we calculated magnetic moments of the six LMZs as a measure of the demagnetization strength and compared the results for all six LMZs (Figure 3e). The magnetic moment is defined as the summation of the reduced magnetization values multiplied by the corresponding volumes of the magnetized layers, i.e., $\sum (\Delta M_i \times V_i)$ [Tivey et al., 1993], assuming a magnetization layer thickness of 500 m in all inversions. The magnetic moment for Area A on the SWIR for Case 1 (with 4 times annihilator) is about $-3 \times 10^7 \text{ Am}^2$ (Figure 3e), similar to that of the New Field vent area on the JdF. The magnetic moment of the TAG area is about $-8 \times 10^7 \text{ Am}^2$. The magnetic moments of the remaining three LMZs (Dante-Grotto, Bastille, and Relict Field) on the JdF vary from -3 to $-5.5 \times 10^7 \text{ Am}^2$. For Area A on the SWIR, we also calculated the moment for Case 2 (with 16 times annihilator) to be about $-16.6 \times 10^7 \text{ Am}^2$ (Figure 3e), which is about twice the value for TAG and five times the value for Case 1 of the SWIR Area A, respectively. Although the different amount of annihilators has produced substantial uncertainties to the results of both area and magnetic moment, the solution for Case 1 can be regarded as the minimum value of the magnetic moment of the low magnetization zone for the Area A on the SWIR.

5. Conclusions

[13] Inversion of near-bottom magnetic data has revealed a well-defined low crustal magnetization zone near a local topographic high on the SWIR with a maximum magnetization reduction of 3 A/m. The first high-temperature hydrothermal vents observed on the SWIR are located directly within or adjacent to this LMZ, indicating that this LMZ may be the result of hydrothermal alteration over a period of time. The area of this LMZ measures at least $6.7 \times 10^4 \text{ m}^2$, which is greater than that of the LMZs for the TAG vent field on the MAR, and four vent areas on the JdF (Relict Field, Bastille, Dante-Grotto, and New Field). The calculated magnetic moment ($-3 \times 10^7 \text{ Am}^2$) is than that of the TAG field on the MAR ($-8 \times 10^7 \text{ Am}^2$) when applying four times annihilator (Case 1). However, if the average magnetization value of the Area A on the SWIR is required to match that of the sea surface magnetization inversion of a larger region (Case 2), the calculated magnetic moment ($-16.6 \times 10^7 \text{ Am}^2$) could be twice as large as that of the TAG and five times that of the Area A Case 1, respectively. In comparison, the magnetic moments of the four individual vent sites on the JdF (ranging from -5×10^7 to $-3 \times 10^7 \text{ Am}^2$) are smaller than that of the TAG, but still of the same magnitude. Together these results indicate that crustal demagnetization is a common feature associated with basalt-hosted hydrothermal vent fields along mid-ocean ridges of all spreading rates. Furthermore, the crustal demagnetization of the Area A on the ultraslow-spreading SWIR is comparable in strength as that of the TAG area on the slow-spreading MAR.

[14] **Acknowledgments.** We are grateful to the crew and scientific party of DY115-19 cruise on board R/V DaYangYiHao and the WHOI ABE group. We also thank Clare Williams for insightful discussion. This work was supported by NSF-China and COMRA Projects 40676023 and DYXM-115-02-03-02 (JZ and YJC), the Charles D. Hollister Endowed Fund for Support of Innovative Research at WHOI (JL), and the ChEss Program of the Census of Marine Life (CRG).

References

- Ade-Hall, J. M., H. C. Palmer, and T. P. Hubbard (1971), The magnetic and opaque petrological response of basalt to regional hydrothermal alteration, *Geophys. J. R. Astron. Soc.*, *24*, 137–174.
- Blakely, R. J. (1996), *Potential Theory in Gravity and Magnetic Applications*, Cambridge Univ. Press, New York.
- Font, L., B. J. Murton, S. Roberts, and A. G. Tindle (2007), Variations in melt productivity and melting conditions along SWIR (70°E–49°E): Evidence from olivine-hosted and plagioclase-hosted melt inclusions, *J. Petrol.*, *48*(8), 1471–1494, doi:10.1093/petrology/egm026.
- Georgen, J., J. Lin, and H. Dick (2001), Evidence from gravity anomalies for interactions of the Marion and Bouvet hotspots with the Southwest Indian Ridge: Effects of transform offsets, *Earth Planet. Sci. Lett.*, *187*, 283–300, doi:10.1016/S0012-821X(01)00293-X.
- German, C. R., D. R. Yoerger, M. Jakuba, T. M. Shank, C. H. Langmuir, and K. Nakamura (2008), Hydrothermal exploration using the *Autonomous Benthic Explorer, Deep Sea Res., Part I*, *55*, 203–219, doi:10.1016/j.dsr.2007.11.004.
- Guspi, F. (1987), Frequency-domain reduction of potential field measurements to a horizontal plane, *Geoexploration*, *24*, 87–98, doi:10.1016/0016-7142(87)90083-4.
- Irving, E. (1970), The Mid-Atlantic Ridge at 45°N. XIV. Oxidation and magnetic properties of basalt; review and discussion, *Can. J. Earth Sci.*, *7*, 1528–1538.
- Johnson, H. P., and T. Atwater (1977), Magnetic study of basalts from the Mid-Atlantic Ridge, lat. 37°N, *Geol. Soc. Am. Bull.*, *88*, 637–647, doi:10.1130/0016-7606(1977)88<637:MSOBF>2.0.CO;2.
- Mendel, V., D. Sauter, C. Rommevaux-Jestin, P. Patriat, F. Lefebvre, and L. M. Parson (2003), Magmato-tectonic cyclicity at the ultra-slow spreading Southwest Indian Ridge: Evidence from variations of axial volcanic ridge morphology and abyssal hills pattern, *Geochem. Geophys. Geosyst.*, *4*(5), 9102, doi:10.1029/2002GC000417.
- Meyzen, C. M., M. J. Toplis, E. Humler, J. N. Ludden, and C. Mevel (2003), A major discontinuity in mantle composition beneath the Southwest Indian Ridge, *Nature*, *421*, 731–733, doi:10.1038/nature01424.
- Parker, R. L., and S. P. Huestis (1974), The inversion of magnetic anomalies in the presence of topography, *J. Geophys. Res.*, *79*, 1587–1593, doi:10.1029/JB079i011p01587.
- Patriat, P., and J. Segoufin (1988), Reconstruction of the central Indian Ocean, *Tectonophysics*, *155*, 211–234, doi:10.1016/0040-1951(88)90267-3.
- Pilkington, M., and W. E. S. Urquhart (1990), Reduction of potential field data to a horizontal plane, *Geophysics*, *55*, 549–555, doi:10.1190/1.1442866.
- Sauter, D., H. Carton, V. Mendel, M. Munsch, C. Rommevaux-Jestin, J.-J. Schott, and H. Whitechurch (2004), Ridge segmentation and the magnetic structure of the Southwest Indian Ridge (at 50°30'E, 55°30'E and 66°20'E): Implications for magmatic processes at ultraslow-spreading centers, *Geochem. Geophys. Geosyst.*, *5*, Q05K08, doi:10.1029/2003GC000581.
- Tao, C., et al. (2007), First discovery and investigation of a high-temperature hydrothermal vent field on the ultraslow spreading Southwest Indian Ridge, *Eos Trans. AGU*, *88*(52), Fall Meet. Suppl., Abstract T52B-07.
- Tivey, M. A., and H. P. Johnson (2002), Crustal magnetization reveals subsurface structure of Juan de Fuca Ridge hydrothermal vent fields, *Geology*, *30*, 979–982, doi:10.1130/0091-7613(2002)030<0979:CMRSSO>2.0.CO;2.
- Tivey, M. A., P. A. Rona, and H. Schouten (1993), Reduced crustal magnetization beneath the active sulfide mound, TAG hydrothermal field, Mid-Atlantic Ridge at 26°N, *Earth Planet. Sci. Lett.*, *115*, 101–115, doi:10.1016/0012-821X(93)90216-V.
- Tivey, M. A., H. Schouten, and M. C. Kleinrock (2003), A near-bottom magnetic survey of the Mid-Atlantic Ridge axis at 26°N: Implication for the tectonic evolution of the TAG segment, *J. Geophys. Res.*, *108*(B5), 2277, doi:10.1029/2002JB001967.
- Watkins, N. D., and T. P. Paster (1971), The magnetic properties of igneous rocks from the ocean floor, *Philos. Trans. R. Soc. London, Ser. A*, *268*, 507–550, doi:10.1098/rsta.1971.0011.
- Y. J. Chen and J. Zhu, Institute of Theoretical and Applied Geophysics, School of Earth and Space Science, Peking University, Beijing 100871, China. (johnyc@pku.edu.cn)
- C. R. German, J. Lin, M. A. Tivey, and D. R. Yoerger, Woods Hole Oceanographic Institution, 360 Woods Hole Rd., Woods Hole, MA 02543, USA.
- C. Tao, Key Laboratory of Submarine Geosciences, Second Institute of Oceanography, State Oceanic Administration, No. 36 Baochubei Rd., Hangzhou 310012, China.